Composite Fe_3O_4–W(100) probes for scanning tunneling microscopy

Sergey I. Bozhko, Sergey V. Chekmazov, Victor Usov, Olaf Lübben, Andrey M. Ionov, Han-Chun Wu, Valery N. Semenov, Maria E. Nesterova, Sergey A. Krasnikov, and Igor V. Shvets

Citation: Journal of Applied Physics **122**, 235301 (2017); doi: 10.1063/1.5001057
View online: https://doi.org/10.1063/1.5001057
View Table of Contents: http://aip.scitation.org/toc/jap/122/23
Published by the American Institute of Physics

Composite Fe_3O_4–W(100) probes for scanning tunneling microscopy

Sergey I. Bozhko,[1,2,a)] Sergey V. Chekmazov,[1,a)] Victor Usov,[2] Olaf Lübben,[2] Andrey M. Ionov,[1] Han-Chun Wu,[2] Valery N. Semenov,[1] Maria E. Nesterova,[1] Sergey A. Krasnikov,[2] and Igor V. Shvets[2]

[1]*Institute of Solid State Physics, Russian Academy of Science, 142432 Chernogolovka, Moscow District, Russia*

[2]*Centre for Research on Adaptive Nanostructures and Nanodevices (CRANN), School of Physics, Trinity College, University of Dublin, Dublin 2, Ireland*

(Received 21 August 2017; accepted 26 November 2017; published online 15 December 2017)

A new two-step technique was developed to fabricate a composite probe for a Scanning Tunneling Microscopy (STM). The first step was to form a flat area on the W(100) surface of several hundred square nanometers or less in an area at the end of a single crystalline tungsten tip. The second step consisted of epitaxial growth of a nanoparticle on this flat area by molecular beam epitaxy. Both atomic resolution imaging on the MoO_2/Mo(110) surface covered with Fe nanoclusters and magnetic contrast on Fe nanoclusters were obtained at $T = 78$ K as an indication of an excellent performance and stability of the composite STM probe. The developed technique of composite probes formation is very promising for the fabrication of probes with the required physical characteristics. *Published by AIP Publishing.* https://doi.org/10.1063/1.5001057

I. INTRODUCTION

Scanning tunneling microscopy (STM) was invented about 30 years ago[1,2] and today, it is one of the most powerful techniques of surface science. Using this technique, investigations can be carried out with an atomic or even electron orbital resolution.[3,4] The shape of an STM probe and its electronic structure determine the scope of information that can be obtained from experiment and therefore are essential for the interpretation of the data. Thus, the development of new methods for fabrication of special probes is one of the most important problems in the advancement of the STM technique.

Pt-Ir alloy wires with a diameter of 0.1–0.5 mm are most commonly used for the preparation of STM probes. The Pt-Ir STM probe is made by simultaneously cutting the wire and pulling it off.[5] The shape of the tip is inspected after each cut using a microscope until the tip appears to have obtained a suitable shape. Such a probe usually has a sharp edge comprising a number of micro tips, with the topmost of them used in STM measurements. However, the drawback of this tip fabrication technique is in non-reproducible tip, as geometry can change from one experiment to another. The Pt-Ir STM tips can also be fabricated using electrochemical polishing in a mixture of electrolytes.[6–9] This technique enables the fabrication of round shaped tips with a radius of curvature of 50–100 nm.

The method of preparation of sharp tips from a thin tungsten wire had been well known and widely used even for many years before an STM was invented. Such tips were used to study the crystal structure of W at atomic scale in a field ion microscope.[10,11] Binnig and Rohrer utilized the same technique to prepare fine tungsten tips for their first STM device.[1,2] Thin polycrystalline tungsten wire suitable for STM tip preparation is both readily available and inexpensive. Numerous papers describe the technique of tungsten STM probe preparation using electrochemical polishing in detail.[6,11–15] Tungsten tips with a radius curvature of <30 nm can be prepared using this technique and are suitable for obtaining an atomic spatial resolution using STM. The main disadvantage of this technique is in the formation of a 10 nm thick contamination layer on the tip surface which consists of W oxides and carbon.[14,16,17] This layer has a relatively low conductivity, resulting in a significant decrease in the tunneling current. Preferably, this layer should be removed from the tip surface *in situ* in an ultra high vacuum (UHV) chamber by resistive heating,[11,18] heating by electron bombardment,[15,17,18,20,21] or by Ne^{+}[19] or Ar^{+} ion sputtering.[16,21,22] Using a combination of these techniques allows one to produce tungsten tips which are stable during STM scanning and routinely demonstrate atomic resolution.[21]

Besides W and Pt-Ir, STM probes have been successfully fabricated from several other materials including single crystals of molybdenum,[23] Ag wire,[24–26] Au wire,[8,27,28] Pt, Ir, Pd, and Rh wires.[8]

At present, it is possible to resolve surface corrugation down to one hundredth of the atomic diameter and even distinguish between atomic orbitals. Much of this progress is largely achieved due to advances in the STM probe manufacturing.

Another important aspect of STM is the development of functionalized probes that could provide information on, e.g., magnetic order on the surface through mechanism of spin-polarized tunneling. The theoretical background for the spin-polarized tunneling was given by Slonczewski[29] who pointed out that the tunneling current flowing between two ferromagnetic films depends on the orientation of their magnetization vectors. This effect was observed experimentally in 1975 in a work by Julliere[30] where he measured a change

a)Authors to whom correspondence should be addressed: bozhko@issp.ac.ru and chekmazov@issp.ac.ru

in the conductance in a Fe-Ge-Co contact in a magnetic field at $T = 4.2$ K. The effect was later also exploited in STM measurements to achieve an atomic resolution with magnetic contrast.[31] A ferromagnetic probe was used to achieve a spin dependent tunneling between a tip and sample.[31–33] A number of ferromagnetic materials, i.e., Ni,[34,35] Co,[36] CoCr,[37] CrO_2,[32,33] were used to fabricate magnetic probes.

The preparation of these probes is based on the deposition of thin ferromagnetic films on the surface of paramagnetic tips.[38] In this case, the direction of the magnetization vector strongly depends on the film's magnetic shape anisotropy which, in turn, depends on the deposited film thickness. Such dependence of the magnetization on thickness was studied extensively for Fe films deposited on W(110)[38–40] and Mo(110)[41] surfaces. In the case of a Co film deposited on the W(001) surface, the film undergoes a phase transition from a *bcc* to a *hcp* lattice at a thickness of 2.7 monolayers (MLs). The easy magnetization axis is hereby parallel to the [100] direction of the substrate.[42] Spin polarization emission studies from Co and Fe films deposited on W [100] and W [111] single crystal tips have been previously published.[43–45]

Minakov and Shvets[31] demonstrated that using antiferromagnetic tips, instead of ferromagnetic ones, can suppress the magnetic coupling between the tip and sample. Thereafter, a number of antiferromagnetic probes, including Cr, MnNi,[35,46] and MnPt, MnAu, MnIr,[46] have been employed in order to achieve spin sensitivity in STM. Antiferromagnetic probes can also be prepared by the deposition of antiferromagnetic thin films onto the STM tip apex.[47,48] The idea of a spin polarized tunneling current in combined ferromagnetic-antiferromagnetic tunnel junction has been previously proposed in Ref. 49.

One of the most promising applications of STM is single electron devices based on the Coulomb blockade phenomena.[50] The theory of single-electron tunneling was first proposed by Averin and Likharev.[51,52] Using the Coulomb blockade, it is possible to control the charge state of a nanosystem with tunnel junctions. In particular, the charge of a nanosized particle isolated from electrodes by tunnel junctions can be changed discretely by tunneling of single electrons.

The realization of such a system via STM, in the form of a "probe-nanoparticle-substrate," where the nanoparticle is separated by two tunnel junctions, has been demonstrated at both low[53–55] and room temperatures.[56–58] Previously, a Coulomb blockade has been used to fabricate a charge sensor by placing a gold nanoparticle at the end of a tungsten STM tip.[59] The sensor, which was sensitive to changes in the electrostatic environment, was used to study the distribution of local charge density on graphene with a high spatial resolution. However, to our knowledge, this is the only publication where nanoparticle placed on the STM tip apex was used as a sensor. Lack of studies using such probes is due to the absence of reproducible reliable technology of the sensor fabrication. STM tip-nanoparticle-substrate surface geometry is also very promising to study the quantum confinement effect in superconductive nanoparticles.[60,61]

Here, we present a new two-step technique based on molecular beam epitaxy (MBE). As the first step, a small flat area is formed at the top of a W single crystal rod with [100] direction along the rod axis. The rod is terminated by a flat area with (001) orientation. As the second step, we grow a nanoparticle at the flat area to ensure the required functional properties of the tip (e.g., to set direction of the probe's magnetic moment or definite charge state of the probe terminating atom). In this particular paper, we complete the tip fabrication by growing a Fe_3O_4 nanoparticle on the flat area of a metal tip by MBE. Magnetite is chosen as a material of the nanoparticle because spin dependent tunnel current is observed in surface studies of Fe_3O_4 by STM.[35,46,62] Therefore, using it, we can create a probe for spin-polarized STM. The [100] direction of the tip coincides with [100] direction of the rod of which the tip is formed that can be crucial for the interpretation of STM data. Since MBE growth enables excellent control of the film crystal structure, its thickness and composition, one can attain the required physical properties at the tip apex such as stoichiometric composition, crystal structure, and orientation of magnetic easy axis. Two main problems that can be encountered in fabricating of composite probes are targeted in the work. The first one is fabrication of a fine flat area of desired crystallographic orientation. The second one is the controlled growth of Fe_3O_4 nanoparticle on the flat area thus formed.

II. EXPERIMENTAL

It is difficult to create a flat area at the top of the tip using a polycrystalline tungsten or alloyed rod, e.g., like Pt-Ir wire used for making conventional STM probes. The reason is that grains in a polycrystalline wire are randomly oriented, making it impossible to determine precisely the crystallographic orientation of the nanosized tip at the apex. Therefore, it is not possible to manufacture such probes in a reproducible way. For this reason, we utilized single crystal tungsten rods, with a flat area at the apex, for the fabrication of tips.

Tungsten single crystals were grown 100 mm long in the [100] direction and 12 mm in diameter using electron-beam floating zone technique under high vacuum conditions.[63] The chemical purity of the crystals was better than 99.95%. For STM probes preparation, W [100] single crystal bars with dimensions of $0.5 \times 0.5 \times 15\,mm^3$ were cut from crystals using an electrospark wire cutting machine, with all planes of the bars close to the {100} planes. To remove the contaminated and damaged layers, the bars underwent electrochemical polishing in 2M aqua solution of NaOH.

The well-known technique of electrochemical polishing was used to prepare sharp tungsten single crystal tips.[5,6,11,12,14,21] A ring made from stainless steel or a noble metal was placed in a glass with the 2M aqua solution of NaOH and used as a cathode. The single crystal W bar was placed in the center of the ring partly immersed in the solution and served as anode [Fig. 1(a)].

The process of electrochemical polishing starts with the application of a DC voltage U in the range of 3.8 to 4.1 V between the ring and the bar. In order to get a flat surface on the tip apex, a part of the W bar immersed in the solution was covered with a protective layer of varnish or Teflon™, as shown in Fig. 1(b). In this case, the electrochemical

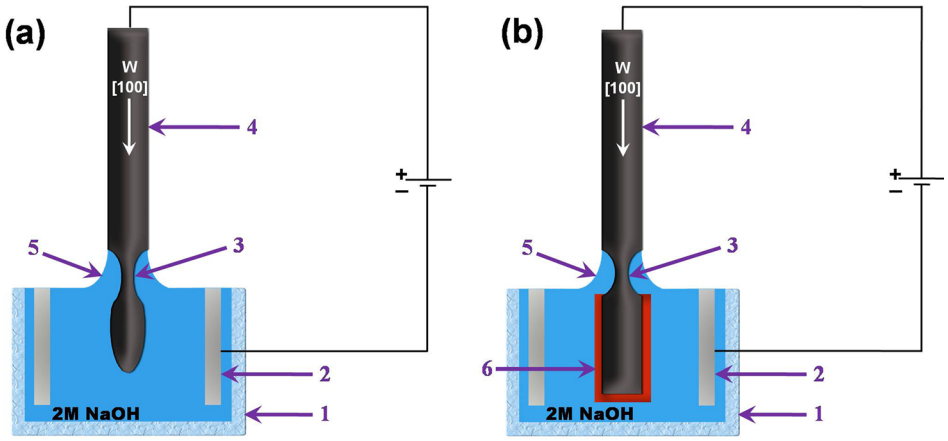

FIG. 1. Schematics of W single crystal tip fabrication: (a)—conventional technique, (b)—the technique using protective bar coverage at the immersed part employed in this study: 1—glass, 2—stainless steel ring, 3—constriction on the bar, 4—W single crystal bar, 5—meniscus, and 6—protective coverage (varnish or Teflon^{TM}).

polishing occurs only at the surface of the electrolyte solution around the meniscus. The length of the immersed part of the rod was in the range of 1–3.5 mm. During the electropolishing process, the constriction diameter decreases continuously until the immersed part below the constriction pulls off under its own weight and forms a desired tip shape. Both the crystal structure orientation and the weight of the immersed bar are vital parameters to achieving a desired tip shape and flat diameter.

The growth of Fe_3O_4 both at the top of the flat apex of STM tip and at W(100) surface was conducted in an MBE chamber with a base pressure of 1×10^{-10} Torr. The sample was annealed at 1000 °C for 2 h in order to remove the surface contamination. Magnetite film 100 ML thick was grown by MBE on the W(100) surface at a deposition rate of 1 ML/s. The details of the growth can be found elsewhere.[64,65]

III. RESULTS AND DISCUSSION

Tungsten single crystals (*bcc* lattice) are brittle and can undergo cleaving along the {100} planes even at room temperature. The dislocations and point defects in a tungsten single crystal grown by electron-beam floating zone technique are created due to very high temperature gradients (axial and radial) and a relatively high cooling rate during crystal growth. The typical value of dislocation density in W single crystals used in our experiments was around 10^5 cm^{-2} (Ref. 63), indicating that the mean distance between the dislocations is about 30 μm. A number of dislocations in a narrow area of constriction are determined by the diameter of the constriction and the density of dislocations. If the constriction diameter becomes smaller than the mean distance between the dislocations, the crystal perfection in this area will be comparable to that of whiskers.[66,67] That is why a comparatively small constriction area can demonstrate brittle fracture under both bending and elongation stresses. When the stress level is large enough, cleaving can proceed in the constriction area, creating a small flat region coinciding with the W(100) plane of a single crystal bar [Figs. 2(a) and 2(b)].

For comparison, a cleaved W(100) fractured constriction area in Figs. 2(a) and 2(b) is shown beside the area created on the top of the conventional tungsten polycrystalline wire [Figs. 2(c) and 2(d)].

The fractured surface in the case of polycrystalline tungsten wire is rougher than the same area of W [100] single crystal bar. For this reason, the latter is much more suitable as a substrate for MBE growth of a nanoparticle which later serves as a sharp nanoscale STM tip.

In our experiments, the constricted region of the single crystal undergoes elongation under stress during the electropolishing process under the weight of the section of the single crystal bar below the constriction. The weight of this section can be easily controlled by changing the initial length of the immersed part.

Figure 3 shows a tungsten single crystal tip with [100] axis and a flat surface at the apex (indicated by yellow arrow). The diameter of the flat region is about ≈130 nm. For this tip, the length of the bar immersed in the electrolyte was 1.5 mm. The flat area on the tip apex is formed when the weight of the bottom part exceeds the value of the tensile stress limit for tungsten, resulting in the crystal in the region of constriction cleaving along (100) planes. Thus, the diameter of the flat area can be controlled by changing the length of the immersed part. The smaller the weight of the part of the rod below the constriction, the less is the diameter of flat tip apex. The weight of the bottom part of 4.6 mg (tensile stress limit of 3.5 GPa) resulted in the creation of a flat area 130 nm in diameter (Fig. 3). The inset in Fig. 4(c) shows the tungsten single crystalline tip with the flat area at the apex of 420 nm in diameter. The Fe_3O_4 nanoparticle was grown on the tip apex.

Prior to the nanoparticle creation on the flat tip apex, we performed experiments on the growth of Fe_3O_4 film on the (100) surface of the single crystal tungsten sample disk 12 mm in diameter and 1.5 mm thick. The film was not homogeneous—the morphology of the film at the periphery of the sample was different from the one at the central area of the sample surface. The growth of the film at the periphery of the sample occurred in accordance with Stranski-Krastanov scenario. Nanoislands 10–200 nm in size were formed on a wetting layer [see Fig. 4(a)]. Figure 4(b) demonstrates the typical SEM image of the film close to the center of the sample disk. The central area of the sample mainly was covered by nanowires up to 50 nm in diameter and up to 2 μm in length. The SEM image of Fe_3O_4 nanoparticle 180 nm thick formed on the tip apex is presented in Fig. 4(c).

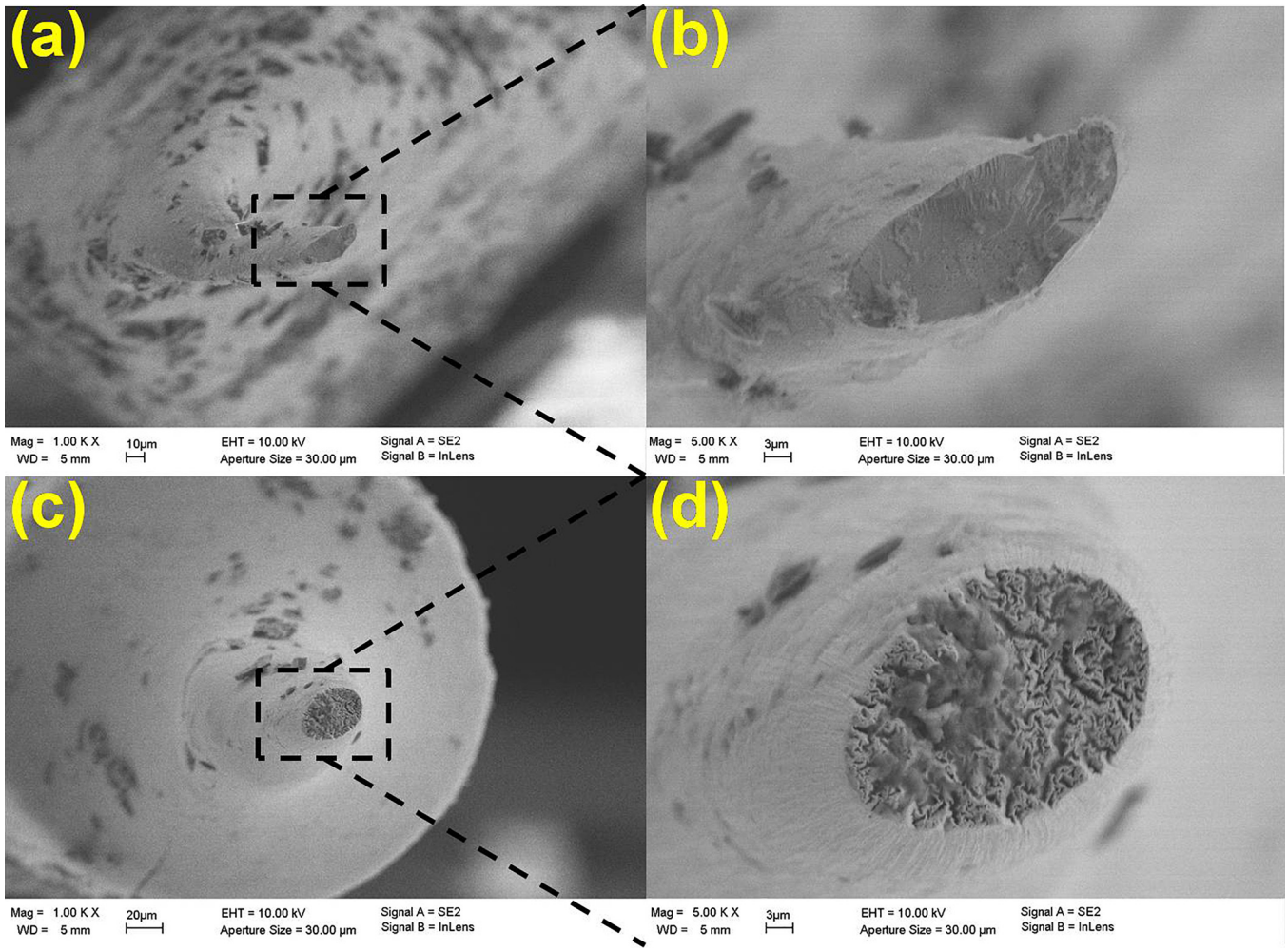

FIG. 2. SEM images of W surfaces in the constricted area: (a) fractured surface of tungsten single crystal bar, (b) the same surface with a higher magnification—the flat area is about $14 \times 34\ \mu m^2$; (c) similar fracture surface for W polycrystalline wire, and (d) the same surface with a higher magnification—the flat area is about $26 \times 36\ \mu m^2$.

As mentioned earlier, magnetite is one of the most promising materials for use in a spin-polarized STM probe.[35,46,62] Fe_3O_4 has a crystallographic structure with two Fe sublattices, *A* and *B*, with magnetic moments antiparallel to each other. The density functional theory calculations[68] and spin resolved photoelectron spectroscopy[69] demonstrated that the density of states (DOS) for the sublattice *A* differs remarkably from that for the *B* sublattice. For example, at the energy of 2 eV below the Fermi level, the DOS is dominated by the *A* sublattice electrons. For this reason, the spin polarization of tunneling current caused by electrons localized in the vicinity of –2 eV should reflect the magnetic ordering of the sublattice *A*, while the electrons localized in the vicinity of 1.3 eV above the Fermi level should link the tunneling current to the sublattice *B*.

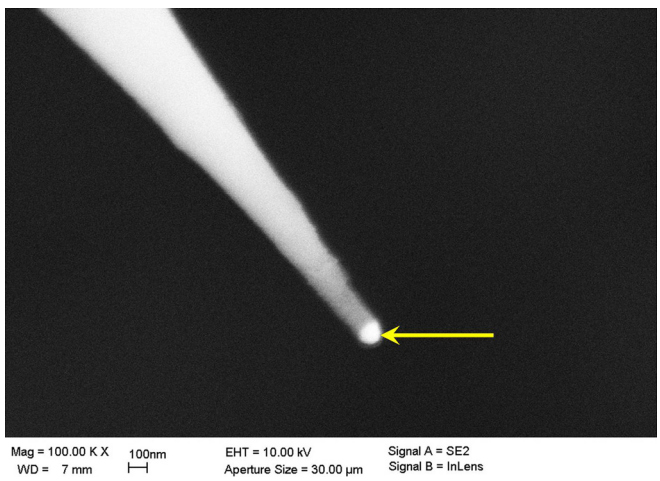

FIG. 3. SEM image of the fracture surface at the tungsten single crystal tip apex.

Imaging capabilities of the tip were demonstrated by conducting the STM measurements in UHV ($p = 2 \times 10^{-11}$ Torr) at 78 K using a commercial STM from Createc. The voltage U_{bias} corresponds to the sample bias with respect to the tip. No drift corrections have been applied to any of the STM images presented in this paper. An ultrathin film of Fe was deposited onto the MoO_2/Mo(110) surface. The MoO_2/Mo(110) surface preparation procedure was previously described in Refs. 70 and 71. The STM image obtained using the composite probe is shown in Fig. 5(a).

Both STM images in Figs. 5(a) and 5(c) of the MoO_2/Mo(110) surface reveal nanorows.[70] The nanorows are 2.3 nm wide and run along the $[1\bar{1}\bar{3}]$ direction [indicated by red arrows in Figs. 5(a) and 5(c)] of the Mo(110) surface.

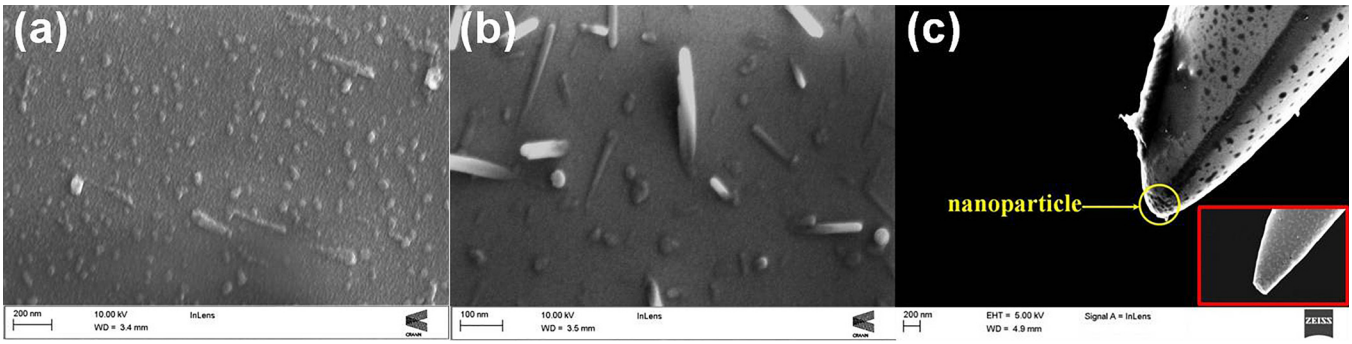

FIG. 4. SEM images of Fe_3O_4 film 100 ML in thick at the periphery (a) and at the center (b) of the W(100) sample. (c) SEM image of W [100] STM tip with a Fe_3O_4 nanoparticle at the tip apex, image of STM tip before Fe_3O_4 nanoparticle deposition is shown in the insert.

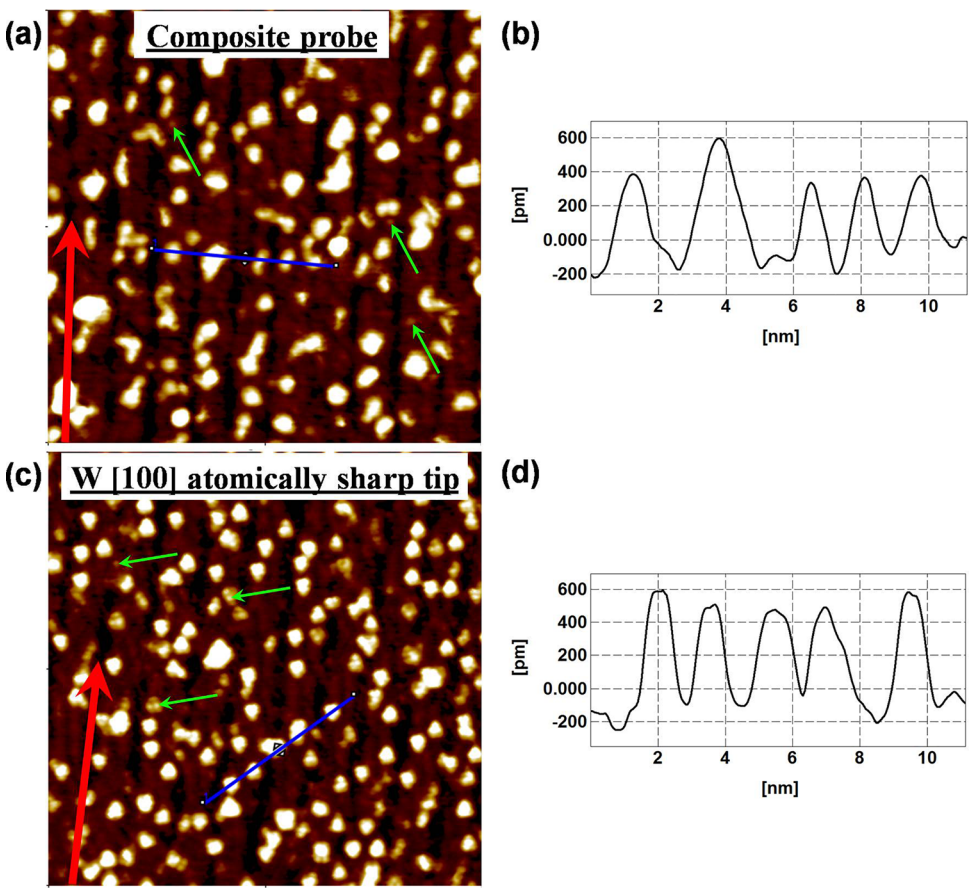

FIG. 5. (a) STM image $26 \times 26\,nm^2$ with 0.2 ML Fe on the surface of MoO_2/Mo(110), obtained using a composite probe. $U_{bias} = -1.8\,V$, $I_{tun} = 400\,pA$. (b) The profile for the flat area taken along the blue line. (c) STM image $26 \times 26\,nm^2$ with 0.2 ML Fe on the surface of MoO_2/Mo(110), taken using an atomically sharp W [100] tip ($U_{bias} = -50\,mV$, $I_{tun} = 3.326\,nA$). (d) The profile for the flat area taken along the blue line. Red arrows indicate nanorows at MoO_2/Mo(110) surface. The nanorows are aligned along the $[1\bar{1}\bar{3}]$ direction of Mo single crystal. Green arrows indicate the individual Fe atoms.

The deposition of Fe on the MoO_2/Mo(110) surface leads to the formation of small nanoclusters, about 12 Å in diameter and 5–6 Å in height [see Figs. 5(b) and 5(d)]. The resolution of individual atoms [indicated by green arrows in Figs. 5(a) and 5(c)] and nanorows in the STM image obtained by a composite probe demonstrates its excellent imaging capabilities. The ultimate resolution achieved with the composite probe is comparable to the resolution in Fig. 5(c) obtained with a common W [100] tip.[21]

Cleaning of the probe by bias voltage pulsing or switching of the tip during scanning resulted in the change of image contrast of some Fe nanoclusters. Figure 6 represents STM images of the same area before and after switching of the probe.

The images of the same Fe clusters indicated by arrows are different in Fig. 6(b) from those in Fig. 6(a). Note that the image in Fig. 6(a) was obtained using a probe after it was transferred from a MBE set-up to a low-temperature STM under ambient conditions. Thus, the probe apex was covered by an adsorbed layer and the probe was not suitable for detecting the spin tunneling through Fe nanoclusters. Bias pulsing or switching of the probe resulted in a cleaning of the tip, revealing the magnetite particle at the end of the probe and making the probe preferentially sensitive to one

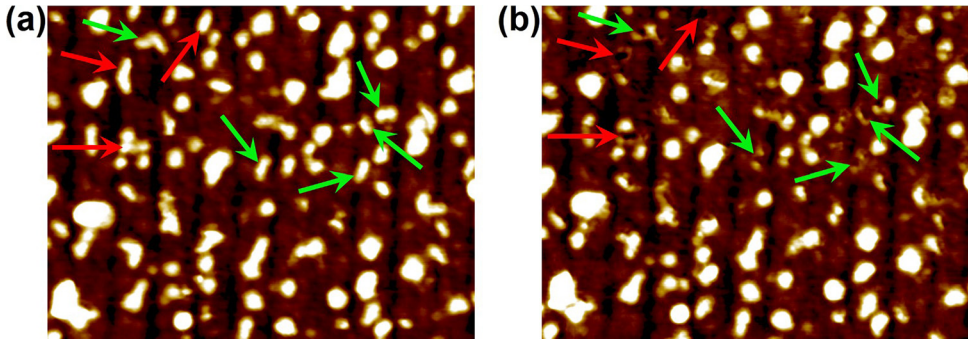

FIG. 6. The same area $26 \times 20.3\,\text{nm}^2$ of Fe nanoclusters on the MoO_2/Mo(110) surface, obtained using a composite probe before (a) and after (b) switching of the probe. $U_{bias} = -2.3$ V and $I_{tun} = 400$ pA.

spin direction [Fig. 6(b)]. Usually, the probe change results in the change of the entire image. In the case of array of clusters, this would change the appearance of all the clusters. In this case, a subset of clusters change, while others remain the same. The subset is not defined by the cluster size; in contrast, there are smaller and larger clusters in each subset. These results confirm that there is a preferential direction of magnetic polarization of nanoclusters and these are imaged by the composite STM probe. However, the negative contrast of nanoclusters indicated by red arrows and the suppressed contrast of nanoclusters indicated by green arrows prove that polarization of some nanoclusters does not coincide with the preferential direction. Note that MoO_2/Mo(110) surface contains a number of nonequivalent sites and, consequently, molecular field responsible for polarization of the nanocluster can be varied for different nanoclusters. In contrast to earlier studies,[71] where Fe nanoclusters on the MoO_2/Mo(110) surface showed superparamagnetic behavior as was measured by X-Ray magnetic circular dichroism at 150 K, our experiments reveal the fixed magnetic polarization of the nanoclusters at 78 K.

IV. CONCLUSION

A method for the fabrication of composite STM probes from single crystalline tungsten is presented. The probe axis was along the W [100] direction. The formation of a small flat area perpendicular to the [100] axis at the tip apex was the main peculiarity resulting from the single crystalline nature of the W bar deployed for making the tip. In contrast to conventional tip fabrication techniques, the bottom part of the tungsten single crystal bar, which is immersed in the electrolyte during the electropolishing, was covered by a protective layer of varnish or Teflon^{TM}. A flat area at the tip apex was achieved by cleaving of the crystal bar along the W(100) plane when the weight of the rod immersed into the electrolyte exceeds the tensile stress limit.

A Fe_3O_4 nanoparticle with the size of 180 nm was grown on the flat top of the probe to form the tip apex. The composite probe demonstrated an excellent stability and atomic resolution in STM experiments performed on the MoO_2/Mo(110) surface covered by Fe nanoclusters. Scanning of the surface using a composite STM probe reveals the magnetic contrast.

ACKNOWLEDGMENTS

This work was partially supported by the RFBR Grant No. 16–02–00727 and the Program of Presidium of Russian Academy of Sciences. The authors thank Dr. A. N. Chaika for fruitful discussions on the STM tip preparation and V. M. Chernyak for technical support.

[1]G. Binnig, H. Rohrer, Ch. Gerber, and E. Weibel, Appl. Phys. Lett. **40**, 178 (1982).
[2]G. Binning, H. Rohrer, Ch. Gerber, and E. Weibel, Phys. Rev. Lett. **49**, 57 (1982).
[3]F. J. Giessibl, H. Bielefeldt, S. Hembacher, and J. Mannhart, Ann. Phys. –Leipzig **10**, 887 (2001).
[4]A. N. Chaika, JETP Lett. **99**, 731 (2014).
[5]C. J. Chen, *Introduction to Scanning Tunneling Microscopy* (Oxford University Press, New York, 2008), pp. 312–329.
[6]A. J. Melmed, J. Vac. Sci. Technol. B **9**, 601 (1991).
[7]B. Zhang and E. Wang, Electrochim. Acta **39**, 103 (1994).
[8]A. J. Nam, A. Teren, T. A. Lusby, and A. J. Melmed, J. Vac. Sci. Technol. B **13**, 1556 (1995).
[9]A. H. Sørensen, U. Hvid, M. W. Mortensen, and K. A. Mørch, Rev. Sci. Instrum. **70**, 3059 (1999).
[10]E. W. Müller and T. T. Tsong, "Principles and applications," *Field Ion Microscopy* (Elsevier, New York, 1969).
[11]W. Paul and P. Grütter, "Field ion microscopy for the characterization of scanning probes," in *Surface Science Tools for Nanomaterials Characterization*, edited by Ch. S. S. R. Kumar (Springer–Verlag, Berlin, Heidelberg, 2015), pp. 159–198.
[12]J. P. Ibe, P. P. Bey, Jr., S. L. Brandow, R. A. Brizzolara, N. A. Burnham, D. P. DiLella, K. P. Lee, C. R. K. Marrian, and R. J. Colton, J. Vac. Sci. Technol. A **8**, 3570 (1990).
[13]R. Zhang and D. G. Ivey, J. Vac. Sci. Technol. B **14**, 1 (1996).
[14]A. I. Olivia, G. A. Romero, J. L. Peña, E. Anguiano, and M. Aguilar, Rev. Sci. Instrum. **67**, 1917 (1996).
[15]I. Ekvall, E. Wahlström, D. Claesson, H. Olin, and E. Olsson, Meas. Sci. Technol. **10**, 11 (1999).
[16]D. K. Biegelsen, F. A. Ponce, J. C. Tramontana, and S. M. Koch, Appl. Phys. Lett. **50**, 696 (1987).
[17]A. Cricenti, E. Paparazzo, M. A. Scarselli, L. Moretto, and S. Selci, Rev. Sci. Instrum. **65**, 1558 (1994).
[18]M. Setvín, J. Javorský, D. Turčinková, I. Matolínová, P. Sobotík, P. Kocán, and I. Ošťádal, Ultramicroscopy **113**, 152 (2012).
[19]S. Ernst, S. Wirth, M. Rams, V. Dolocan, and F. Steglich, Sci. Technol. Adv. Mater. **8**, 347 (2007).
[20]Z. Q. Yu, C. M. Wang, Y. Du, S. Tsevuthasan, and I. Lyubinetsky, Ultramicroscopy **108**, 873 (2008).
[21]A. N. Chaika, N. N. Orlova, V. N. Semenov, E. Yu. Postnova, S. A. Krasnikov, M. G. Lazarev, S. V. Chekmazov, V. Yu. Aristov, V. G. Glebovsky, S. I. Bozhko, and I. V. Shvets, Sci. Rep. **4**, 3742 (2014).
[22]K. N. Eltsov, V. M. Shevlyuga, V. Yu. Yurov, A. V. Kvit, and M. S. Kogan, Phys. Low–Dimens. Struct. **9/10**, 7 (1996).
[23]S. Morishita and F. Okuyama, J. Vac. Sci. Technol. A **9**, 167 (1991).
[24]A. A. Gorbunov, B. Wolf, and J. Edelmann, Rev. Sci. Instrum. **64**, 2393 (1993).

[25]K. Dickmann, F. Demming, and J. Jersch, Rev. Sci. Instrum. **67**, 845 (1996).
[26]M. Iwami, Y. Uehara, and S. Ushioda, Rev. Sci. Instrum. **69**, 4010 (1998).
[27]M. C. Baykul, Mater. Sci. Eng. B –Solid **74**, 229 (2000).
[28]B. Ren, G. Picardi, and B. Pettinger, Rev. Sci. Instrum. **75**, 837 (2004).
[29]J. C. Slonczewski, Phys. Rev. B **39**, 6995 (1989).
[30]M. Julliere, Phys. Lett. A **54**, 225 (1975).
[31]A. A. Minakov and I. V. Shvets, Surf. Sci. Lett. **236**, L377 (1990).
[32]R. Wiesendanger, H.-J. Güntherodt, G. Güntherodt, R. J. Gambino, and R. Ruf, Phys. Rev. Lett. **65**, 247 (1990).
[33]S. N. Molotkov, Surf. Sci. **261**, 7 (1992).
[34]M. Cavallini and F. Biscarini, Rev. Sci. Instrum. **71**, 4457 (2000).
[35]S. F. Ceballos, G. Mariotto, S. Murphy, and I. V. Shvets, Surf. Sci. **523**, 131 (2003).
[36]C. Albonetti, I. Bergenti, M. Cavallini, V. Dediu, M. Massi, J.-F. Moulin, and F. Biscarini, Rev. Sci. Instrum. **73**, 4254 (2002).
[37]R. Allenspach, H. Salemink, A. Bischof, and E. Weibel, Z. Phys. B: Condens. Matter **67**, 125 (1987).
[38]M. Bode, R. Pascal, and R. Wiesendanger, J. Vac. Sci. Technol. A **15**, 1285 (1997).
[39]R. Wiesendanger and M. Bode, Solid State Commun. **119**, 341 (2001).
[40]M. Bode, Rep. Prog. Phys. **66**, 523 (2003).
[41]J. Prokop, A. Kukunin, and H. J. Elmers, Phys. Rev. B **73**, 014428 (2006).
[42]W. Wulfhekel, T. Gutjahr-Löser, F. Zavaliche, D. Sander, and J. Kirschner, Phys. Rev. B **64**, 144422 (2001).
[43]R. Bryl and M. S. Altman, J. Appl. Phys. **94**, 4670 (2003).
[44]A. Kubetzka, P. Ferriani, M. Bode, S. Heinze, G. Bihlmayer, K. von Bergmann, O. Pietzsch, S. Blügel, and R. Wiesendanger, Phys. Rev. Lett. **94**, 087204 (2005).
[45]Y. R. Niu and M. S. Altman, Surf. Sci. **604**, 1055 (2010).
[46]I. V. Shvets, R. Wiesendanger, D. Bürgler, G. Tarrach, H.-J. Güntherodt, and J. M. D. Coey, J. Appl. Phys. **71**, 5489 (1992).
[47]A. Kubetzka, M. Bode, O. Pietzsch, and R. Wiesendanger, Phys. Rev. Lett. **88**, 057201 (2002).
[48]A. Wachowiak, J. Wiebe, M. Bode, O. Pietzsch, M. Morgenstern, and R. Wiesendanger, Science **298**, 577 (2002).
[49]I. V. Shvets, A. N. Grigorenko, K. S. Novoselov, and D. J. Mapps, Appl. Phys. Lett. **86**, 212501 (2005).
[50]H. R. Zeller and I. Giaever, Phys. Rev. **181**, 789 (1969).
[51]D. V. Averin and K. K. Likharev, J. Low Temp. Phys. **62**, 345 (1986).
[52]D. V. Averin and K. K. Likharev, "Single electronics: A correlated transfer of single electrons and Cooper pairs in systems of small tunnel junctions," in *Mesoscopic Phenomena in Solids*, edited by B. L. Altshuler, P. A. Lee, and R. A. Webb (Elsevier Science Publishers B. V., Amsterdam, 1991), pp. 173–272.
[53]Z. Y. Rong, L. F. Cohen, and E. L. Wolf, Phys. Lett. A **146**, 281 (1990).
[54]M. Amman, S. B. Field, and R. C. Jaklevic, Phys. Rev. B **48**, 12104 (1993).
[55]H. van Kempen, J. G. A. Dubois, J. W. Gerritsen, and G. Schmid, Physica B **204**, 51 (1995).
[56]F. Kreupl, J. Vancea, L. Risch, F. Hofmann, and H. Hoffmann, Microelectron. Eng. **30**, 451 (1996).
[57]H. Graf, J. Vancea, and H. Hoffmann, Appl. Phys. Lett. **80**, 1264 (2002).
[58]G. Yang, L. Tan, Y. Yang, S. Chen, and G.-Y. Liu, Surf. Sci. **589**, 129 (2005).
[59]A. Deshpande, W. Bao, Z. Zhao, C. N. Lau, and B. J. LeRoy, Phys. Rev. B **83**, 155409 (2011).
[60]T. Cren, L. Serrier-Garcia, F. Debontridder, and D. Roditchev, Phys. Rev. Lett. **107**, 097202 (2011).
[61]S. Vlaic, S. Pons, T. Zhang, A. Assouline, A. Zimmers, C. David, G. Rodary, J.-C. Girard, D. Roditchev, and H. Aubin, Nat. Commun. **8**, 14549 (2017).
[62]N. Berdunov, S. Murphy, G. Mariotto, and I. V. Shvets, Phys. Rev. Lett. **93**, 057201 (2004).
[63]V. G. Glebovsky, V. N. Semenov, and V. V. Lomeyko, J. Cryst. Growth **87**, 142 (1988).
[64]S. K. Arora, H.-C. Wu, R. J. Choudhary, I. V. Shvets, O. N. Mryasov, H. Yao, and W. Y. Ching, Phys. Rev. B **77**, 134443 (2008).
[65]Y. Zhou, X. Jin, and I. V. Shvets, J. Appl. Phys. **95**, 7357 (2004).
[66]S. S. Brenner, J. Appl. Phys. **27**, 1484 (1956).
[67]E. M. Nadgornyĭ, Yu. A. Osip'yan, M. D. Perkas, and V. M. Rozenberg, Sov. Phys. Usp. **2**, 282 (1959).
[68]Z. Zhang and S. Satpathy, Phys. Rev. B **44**, 13319 (1991).
[69]J. G. Tobin, S. A. Morton, S. W. Yu, G. D. Waddill, I. K. Schuller, and S. A. Chambers, J. Phys. –Condens. Matter **19**, 315218 (2007).
[70]K. Radican, N. Berdunov, G. Manai, and I. V. Shvets, Phys. Rev. B **75**, 155434 (2007).
[71]O. Lübben, S. A. Krasnikov, A. B. Preobrajenski, B. E. Murphy, S. I. Bozhko, S. K. Arora, and I. V. Shvets, J. Appl. Phys. **111**, 07B515 (2012).